



Is the Lunar Magnetic Field Correlated With Gravity or topography?

Shengxia Gong, Mark Wieczorek

► To cite this version:

Shengxia Gong, Mark Wieczorek. Is the Lunar Magnetic Field Correlated With Gravity or topography?. Journal of Geophysical Research. Planets, 2020, 125 (4), 10.1029/2019JE006274 . hal-02980430

HAL Id: hal-02980430

<https://hal.science/hal-02980430>

Submitted on 23 Jun 2022

HAL is a multi-disciplinary open access archive for the deposit and dissemination of scientific research documents, whether they are published or not. The documents may come from teaching and research institutions in France or abroad, or from public or private research centers.

L'archive ouverte pluridisciplinaire **HAL**, est destinée au dépôt et à la diffusion de documents scientifiques de niveau recherche, publiés ou non, émanant des établissements d'enseignement et de recherche français ou étrangers, des laboratoires publics ou privés.

Copyright

Key Points:

- The origin of lunar magnetic anomalies is investigated through a correlation analysis with gravity and topography
- About 11% of the surface shows correlations with surface topography that may be iron-rich impact ejecta
- About 4% of the surface shows correlations with density anomalies deep beneath the surface

Supporting Information:

- Supporting Information S1

Correspondence to:

S. Gong,
 sxgong@shao.ac.cn

Citation:


Gong, S., & Wieczorek, M. A. (2020). Is the lunar magnetic field correlated with gravity or topography? *Journal of Geophysical Research: Planets*, 125, e2019JE006274. <https://doi.org/10.1029/2019JE006274>

Received 8 NOV 2019

Accepted 27 MAR 2020

Accepted article online 15 APR 2020

Is the Lunar Magnetic Field Correlated With Gravity or topography?

Shengxia Gong^{1,2}  and Mark A. Wieczorek² 

¹CAS Key Laboratory of Planetary Sciences, Shanghai Astronomical Observatory, Chinese Academy of Sciences, Shanghai, China, ²Université Côte d'Azur, Observatoire de la Côte d'Azur, CNRS, Laboratoire Lagrange, Nice, France

Abstract Magnetic field measurements made from orbit show that there are strong magnetic anomalies on the Moon, but many of these show no clear correlation with known geological processes. Given that the primary magnetic carrier on the Moon is metallic iron, which is considerably denser than the silicate minerals that make up the crust, we might expect that there would be a correlation between the magnetic field and gravity. If the magnetic anomaly were related to iron-rich impact ejecta, there might also be a correlation between the magnetic field and topography. We use magnetic field, topography, and gravity data to test whether such correlations exist. Our results demonstrate that some magnetic anomalies show statistically significant positive correlations with free-air gravity and topography, and the magnetic sources within these regions could potentially be iron-rich impact ejecta. In a few cases, the magnetic anomalies show statistically significant positive correlations with Bouguer gravity, implying that the magnetic anomalies are associated with density anomalies within either the crust or upper mantle. The origin of the vast remainder of lunar magnetic anomalies remains enigmatic.

Plain Language Summary Although the Moon does not have a global magnetic field like the Earth at the present time, portions of the lunar crust are found to be strongly magnetized. The origin of these crustal magnetic anomalies is uncertain since many of these anomalies show no clear correlation with geological features. Here we test whether these magnetic anomalies are related to topography or gravity in order to constrain the origin of these anomalies. We found that in some cases, the magnetic anomalies could be related to iron-rich impact ejecta. In a smaller number of cases, some magnetic anomalies might be related to subsurface density anomalies.

1. Introduction

The Moon does not have a core-generated magnetic field at present, but surface and orbital magnetic field measurements show that portions of the lunar crust are strongly magnetized (Dyal et al., 1974; Hood et al., 2001; Tsunakawa et al., 2010). Some lunar samples collected on the Moon's surface also are magnetized, and paleomagnetic analyses of these samples suggest that a long-lived core dynamo could have operated from ~4.25 Ga (Garrick-Bethell et al., 2009, 2017) to somewhere between ~2.5 and 1 Ga (Mighani et al., 2020; Tikoo et al., 2017). The surface intensity of this early dynamo field is predicted to be 10s of μT and to have decreased by an order of magnitude after 3.56 Ga (Suavet et al., 2013; Tikoo et al., 2014). Several mechanisms have been proposed to drive a core dynamo, including thermal and thermochemical convection (Evans et al., 2014; Konrad & Spohn, 1997; Laneuville et al., 2014; Scheinberg et al., 2015), and mechanical forcing by precession, librations, and non-synchronous rotation (Cébron et al., 2019; Dwyer et al., 2011; Le Bars et al., 2011). Recently, a dynamo generated by convection in a silicate basal magma ocean has also been proposed to explain the early lunar magnetic field (Scheinberg et al., 2018).

The lunar magnetic anomalies almost certainly formed in the presence of a long-lived magnetic field (for a review, see Weiss & Tikoo, 2014). However, it is unclear as to whether these magnetic anomalies formed at the same time as the primordial crust or later as a result of subsequent geological processes. Though some of the magnetic sources could be related to lateral variations in iron metal content of the primordial crust, others could be related to metal-rich basin impact ejecta, basin impact melt sheets, ancient lava flows, or magmatic intrusions (Halekas et al., 2001; Hemingway & Tikoo, 2018; Hood, 2011; Hood & Artemieva, 2008; Oliveira et al., 2017; Purucker et al., 2012; Wieczorek, 2018; Wieczorek et al., 2012). One of the key difficulties

in distinguishing among these hypotheses is that the vast majority of these anomalies show no clear correlations with known geological processes. A few exceptions to this rule do exist. The impact melt sheets of about six Nectarian basins (Serenitatis, Crisium, Humboldtianum, Moscoviense, Mendel-Rydberg, and Nectaris) are clearly magnetized (Le Bars et al., 2011; Oliveira et al., 2017), as is the northern rim of the pre-Nectarian South Pole-Aitken basin (Wieczorek et al., 2012). Recently, Reiner Gamma has also been suggested to be potentially a magnetized impact melt sheet that was later buried by mare basalts (Garrick-Bethell & Kelley, 2019). These observations could be accounted for by the incorporation of small quantities of iron metal derived from the projectile in these deposits. The iron metal would then have subsequently magnetized in the presence of a core generated dynamo field as the melt sheet crystallized and cooled.

Lunar magnetic anomalies are likely related in some way to changes in the composition of the crust. As the crustal composition is related to its density, lunar magnetic anomalies might be expected to have a gravitational signature. One possible scenario involves magnetic materials that are located deep below the surface. As one example, basaltic and Mg-suite plutonic rocks could have acquired a thermoremanent magnetization as they cooled in the presence of a long-lived magnetic field. These mafic rocks are intrinsically more dense than the anorthositic crust that they intruded (e.g., Wieczorek et al., 2001), and their density contrast with the surrounding crust could potentially be enhanced by having comparatively less impact-generated porosity as a result of their younger ages. These rocks could thus generate both a magnetic anomaly and a positive Bouguer gravity anomaly, but they would not be expected to be associated with topography. (As will be discussed in section 2, the Bouguer anomaly is the gravitational attraction after removing the gravitational contribution of topography.) Another example is that the compositional anomalies in the deep crust could have formed at the same time as the crust itself, which would probably again generate both magnetic anomalies and Bouguer gravity anomalies, but would not be associated with topography.

A second scenario is that the magnetic materials were emplaced, or formed, on the surface. For example, the impact melt pool of an impact basin might be enriched in iron metal that was derived from the impactor, and it could potentially acquire a strong remanent magnetization if it cooled in the presence of a magnetic field (e.g., Garrick-Bethell & Kelley, 2019; Oliveira et al., 2017). The composition of the impact melt pool would likely differ from the surrounding crust, either as a result of differentiation during crystallization or by being derived from deep crustal and mantle materials. Furthermore, the melt sheet would initially form with no porosity, which is considerably different from the ~12% porosity that is found in typical upper crustal highland rocks (Wieczorek et al., 2013). In addition to potentially having a correlation with Bouguer gravity (from the variations in crustal density), we might also expect to see a negative correlation with topography given that the impact melt pool is located in the center of the crater where the elevations are lowest. Conversely, magnetized iron-rich impact ejecta deposits surrounding a basin would be expected to exhibit a positive correlation with topography given that they were emplaced directly on top of the preexisting crust.

In this study, we investigate whether the magnetic field of the Moon is correlated with the Bouguer gravity, free-air gravity, or topography. Whereas other studies have noted potential correlations between the magnetic and gravitational fields by inspection of these data in the space domain (such as in the studies of Smrekar et al., 2004, and Milbury et al., 2007, for Mars), we investigate potential correlations using a localized spectral analysis approach. We then quantify the significance of any such correlations using Monte Carlo simulations. In the following section, we describe the data sets that will be employed in our investigation and the localized spectral correlation analysis procedures. Following this, we present our results and then finally discuss the implications of our results for the origin of lunar magnetic anomalies.

2. Data and Methods

The primary data sets used in this study are spherical harmonic models of the Moon's magnetic field, free-air gravity, Bouguer gravity, and topography. The global crustal magnetic field model is a 450 degree and order spherical harmonic model (Tsunakawa et al., 2015) based on both Lunar Prospector and Kaguya measurements. The topography model is a 2500 degree and order spherical harmonic expansion (Wieczorek, 2015) of gridded Lunar Orbiter Laser Altimeter data (Smith et al., 2010). The free-air gravity model is the 900 degree and order spherical harmonic model GRGM900C of Lemoine et al. (2014) that is based on data obtained from the Gravity Recovery and Interior Laboratory mission (Zuber et al., 2013). Lastly, we will make use of a gravity model from Wieczorek et al. (2013) that is the gravity that remains after removing all known gravitational contributions, including topography, long-wavelength variations in crustal density, and long-wavelength

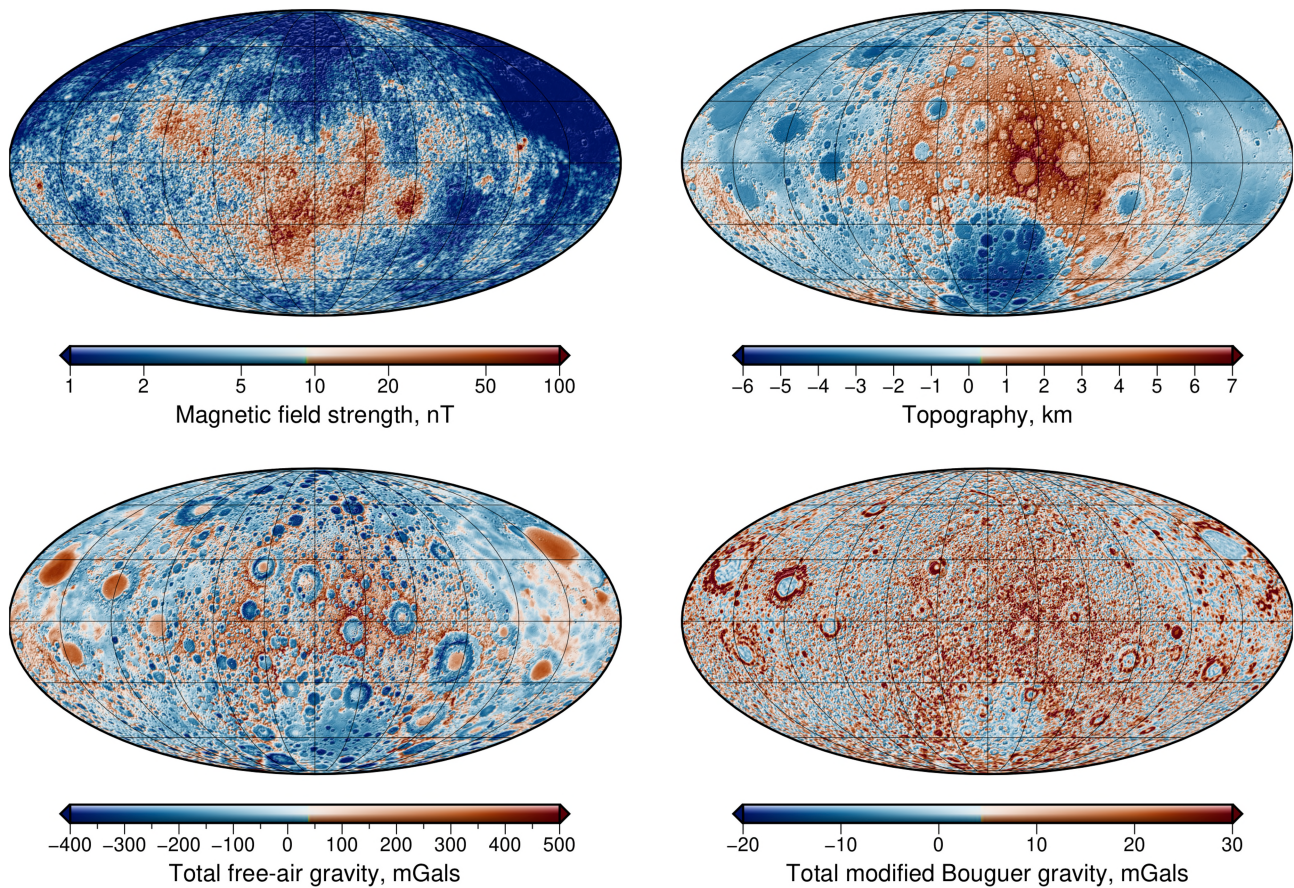


Figure 1. (upper left) Total magnetic field strength, (upper right) topography, (lower left) total free-air gravity, and (lower right) total modified Bouguer gravity of the Moon at the mean planetary radius. All the maps were evaluated using spherical harmonic coefficients up to degree and order 449. Total magnetic field strength is plotted using a logarithmic color scale. All maps are presented in a Mollweide equal-area projection centered over the farside hemisphere on 180° E longitude with grid lines, plotted every 30° in both latitude and longitude.

variations of crustal thickness. The remaining gravitational signal should be the result of short-wavelength density variations within either the crust or upper mantle that differ from the assumed values. This gravity model was previously used in the study by Thorey et al. (2015) and is very similar to the filtered Bouguer gravity model used by Jansen et al. (2017). We will, from this point onward, refer to this gravity model as the “modified Bouguer gravity.” In practice, this gravity product is most similar to the “isostatic anomaly,” with the main difference being that our crustal thickness model is not necessarily isostatic.

The surface crustal magnetic field model of Tsunakawa et al. (2015) was first downward continued to the mean planetary radius ($\sim 1,737.2$ km) which is slightly lower than the reference radius of the model (1,737.4 km). The three vector components, total field intensity, and magnetic potential were then obtained from the Gauss coefficients using the software package SHTOOLS (Wieczorek & Meschede, 2018), with a maximum spherical-harmonic degree of 449 that corresponds to a spatial resolution of 0.2° . In our baseline analyses, we make use of the total magnetic field strength as opposed to any vector component or magnetic potential, as it is the least sensitive to the (unknown) direction of magnetization. The gravity models were also expanded on the same reference sphere. The total free-air gravity and total modified Bouguer gravity were computed from the three vector components of these fields in order to be consistent with the employed total magnetic field intensity. The resulting total magnetic field strength (plotted using a logarithmic color scale), the total free-air gravity, and the total modified Bouguer gravity are plotted in Figure 1 along with the surface topography.

We next performed a cross-correlation analysis to determine if the magnetic field strength was statistically correlated with any of the other three data sets. One approach would be to do the correlation analysis in the spatial domain by determining a single correlation coefficient using data within a specified region of

interest. However, such an analysis would be biased by the longest wavelength signals that usually have the highest amplitudes. To avoid this problem, we instead performed the correlation analyses in the spectral domain, which provides a correlation coefficient for each spherical harmonic degree.

In order to obtain estimates of the spectral correlation that are localized to a region of interest, we employed the multitaper spectrum analysis technique as developed by Wiczorek and Simons (2005, 2007). The idea of this technique is simple: The data are multiplied by one or several specially constructed orthogonal localization windows, and the resulting functions are expanded into spherical harmonics. The spherical harmonic expansion of the localized field $B = hb$, where h is the window and b is the global field, is given by

$$B(\theta, \phi) = h(\theta, \phi) b(\theta, \phi) = \sum_{l=0}^{l_{\max}} \sum_{m=-l}^l B_{lm} Y_{lm}(\theta, \phi), \quad (1)$$

where the localized spherical harmonic coefficients of degree l and order m are given by B_{lm} , Y_{lm} are the corresponding 4π -normalized spherical harmonic functions at colatitude θ and longitude ϕ , and the sum is performed over all degrees that are permissible by the resolution of the data. For a single localization window, the localized auto-power spectrum of the function B is given by

$$S_{BB}(l) = \sum_{m=-l}^l B_{lm}^2, \quad (2)$$

and the localized cross-power spectrum of two function B and G is

$$S_{BG}(l) = \sum_{m=-l}^l B_{lm} G_{lm}. \quad (3)$$

From these two definitions, the localized correlation spectrum can be computed as

$$\gamma(l) = \frac{S_{BG}(l)}{\sqrt{S_{BB}(l) S_{GG}(l)}}. \quad (4)$$

The spectral correlation has a maximum value of 1 when the two fields are perfectly correlated and a minimum value of -1 when they are perfectly anticorrelated. If the two fields were unrelated, the spectral correlation would be close to zero. When multiple localization windows are employed, the localized power spectrum is defined as the average of the spectra from each of the individual localization windows. The correlation estimate is then computed according to equation (4). Our localized spectral analyses make use of the procedures available in the SHTOOLS software package, with all spherical harmonic coefficients converted to the geodesy 4π -normalization.

In order to test whether the two data sets are correlated or not, we define a single statistic that is the average correlation over the degree range of interest:

$$\bar{\gamma} = \frac{1}{l_2 - l_1 + 1} \sum_{l=l_1}^{l_2} \gamma(l), \quad (5)$$

where l_1 and l_2 are the minimum and maximum degrees that will be used in the analyses, respectively. As opposed to statistics that make use of γ^2 , this statistic allows us to investigate the sign of the correlation, and we will discuss later how l_1 and l_2 are chosen.

Given that a high correlation could occur by chance, we next quantified the probability that a specific value of $\bar{\gamma}$ would occur if the two data sets were unrelated to each other using a Monte Carlo approach. Treating the spherical harmonic coefficients of the magnetic field as a random Gaussian process, we created synthetic magnetic field models that are consistent with the localized magnetic power spectrum. First, for a given analysis region, the localized power spectrum of the magnetic potential S_{UU} was computed on the reference sphere of the magnetic field model. The degree-dependent variance of the magnetic field coefficients (using 4π -normalized harmonics) is given by (see equation (11) of Wiczorek, 2018)

$$\langle g_{lm}^2 \rangle = \frac{S_{UU}}{a^2(2l+1)}, \quad (6)$$

where g_{lm} are the Gauss coefficients of the magnetic field and a is the reference radius. For each degree, the spherical harmonic coefficients were chosen to be random Gaussian variables with a variance given by equation (6). After converting the coefficients to the Schmidt semi-normalization, a map of the magnetic field intensity was computed, and the average localized correlation $\bar{\gamma}$ with the secondary field was determined. By repeating this procedure 1,000 times, we constructed a normalized probability distribution of the values of $\bar{\gamma}$ and determined the 95% confidence limits. Any average correlation outside of the 95% confidence limits was considered to be statistically significant given its possibility of occurrence is only 5%. We note that the probability distribution of $\bar{\gamma}$ was found to be symmetric about zero, and for convenience, we used the absolute value of $\bar{\gamma}$ in our Monte Carlo computations.

As described by Wieczorek and Simons (2005), each degree l of the localized spectrum contains contributions from degree $l - l_{\text{win}}$ to $l + l_{\text{win}}$ of the global fields, where l_{win} is the bandwidth of the localization window. This places strict constraints on the degree range of the localized fields that can be analyzed. In particular, we note that when doing the Monte Carlo simulations, the localization window is effectively applied twice to the random realization and that the first $2l_{\text{win}}$ coefficients are hence unreliable. Specifically, the first l_{win} degrees of the localized power spectrum S_{UU} are unreliable as a result of these degrees having wavelengths that are larger than the analysis region. When a random realization is constructed based on this spectrum, and it is itself localized, localized degrees less than $2l_{\text{win}}$ will be affected by the initially unreliable coefficients with degrees less than l_{win} . Thus, the average correlation $\bar{\gamma}$ obtained from the Monte Carlo simulations should be analyzed only for degrees greater than $2l_{\text{win}}$. In a similar manner, the maximum degree that can be analyzed when localizing a random realization based on the localized power spectrum S_{UU} is $l_{\text{max}} - 2l_{\text{win}}$.

When the power spectrum is red (i.e., the power spectrum decreases with the increasing degree), the expectation of the localized power spectrum will be biased with respect to the global one, especially at the lowest degrees. Numerical simulations show that the degree range with substantial bias is usually confined to degrees less than about $2l_{\text{win}}$ (e.g., Simons et al., 2006; Wieczorek & Simons, 2007). Thus, for our simulations, when localizing a random realization of the magnetic field, we will only analyze degrees greater than $3l_{\text{win}}$. Therefore, in our analyses using equation (5), the minimum degree l_1 is set to $3l_{\text{win}}$, and the maximum degree l_2 is set to $l_{\text{max}} - 2l_{\text{win}}$.

3. Results

We calculated localized correlation spectra between the total magnetic field intensity and three separate data sets: topography, total free-air gravity, and total modified Bouguer gravity. In the multitaper analysis, we use only well-localized windows that concentrate 99% of their power within the region of interest. For our baseline results, we chose the localization region to be a spherical cap with an angular radius of 10° (~ 300 km) and set the spectral bandwidth to 26, which provides only one well-localized window. Localized correlation analyses were performed on an equally spaced grid that covered the lunar surface with a 2° grid spacing at the equator. The statistic $\bar{\gamma}$ was computed for each location, and this value was subsequently compared with the 95% confidence limits obtained from Monte Carlo simulations. Regions where the average correlation $\bar{\gamma}$ is higher than would occur by chance at the 95% level were then retained as being statistically significant. Given the manner by which we define statistical significance, if two data sets were unrelated, 5% of the analyses should show average correlations that are significant at the 95% level (2.5% with positive values and 2.5% with negative values).

Figure 2 illustrates how we determined the 95% confidence limits of the $\bar{\gamma}$ statistic, here referred to as $|\bar{\gamma}_{95}|$. In the first panel, we plot a representative localized power spectrum of the magnetic field intensity centered at (30° S, 180° E). This analysis region is on the farside of the Moon in the South Pole-Aitken basin and has higher power at all degrees when compared to the global magnetic power spectrum as plotted in blue. The power spectra of 20 synthetic fields derived from the localized spectrum are plotted in gray. The second panel shows the probability density function of the statistic $\bar{\gamma}$ based on 1,000 synthetic fields. As shown in the figure, the distribution is centered on zero and is Gaussian in form. For this analysis, $|\bar{\gamma}_{95}|$ is close to 0.1: Any value of $|\bar{\gamma}|$ that is greater than this value would occur by chance with a probability of only 5%. Similar Monte Carlo simulations were performed on a map with a grid spacing of 30° in both latitude and longitude. As shown in the third panel, the values of $|\bar{\gamma}_{95}|$ vary across the surface of the Moon only from 0.07 to 0.10. For computation convenience, observed values of $|\bar{\gamma}|$ were compared with the closest value of $|\bar{\gamma}_{95}|$ on this map. We note that the distribution of $\bar{\gamma}$ is not always perfectly centered on zero, which is a result of the small

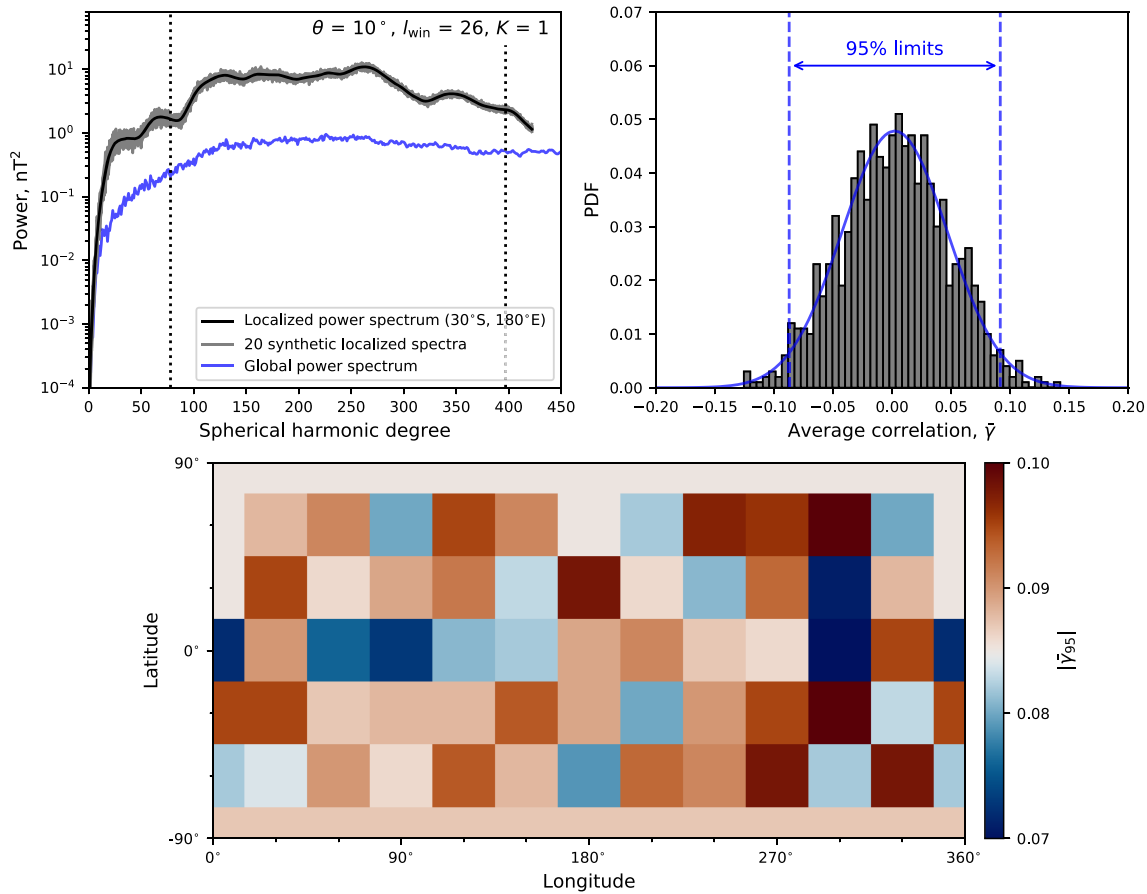


Figure 2. (upper left) Localized magnetic power spectrum at (30° S, 180° E) using a single taper, 20 synthetic power spectra based on this spectrum, and the global magnetic power spectrum of the Moon, all at the mean planetary radius. The vertical dotted lines correspond to the minimum and maximum degrees used in the analyses, which are $3l_{\text{win}}$ and $l_{\text{max}} - 2l_{\text{win}}$, respectively. (upper right) The probability distribution of the average localized correlation \bar{r} between the magnetic field intensity and total free-air gravity using 1,000 synthetic magnetic fields. The dashed blue lines show the 95% confidence limits $|\bar{r}_{95}|$, which is here equal to about 0.1. (bottom) Map of $|\bar{r}_{95}|$ calculated on a 30° grid in latitude and longitude.

number of Monte Carlo simulations that were employed. Nevertheless, tests using different \bar{r}_{95} limits for positive and negative correlations were found to be almost identical to those of using a single value of $|\bar{r}_{95}|$. For convenience, we thus used a single $|\bar{r}_{95}|$ value in the following analyses.

We start by discussing the correlation results between the total magnetic field strength and topography. We plot in Figure 3 (upper right panel) those regions where $|\bar{r}|$ is greater than the 95% confidence limit. We found that 14.7% of the surface area of the Moon possessed average correlations that exceeded the 95% confidence limits; 13.4% of our analyses possessed positive correlations (plotted in red) whereas 1.3% possessed negative correlations (plotted in black). The regions with negative correlations that exceeded the 95% confidence limits are roughly consistent with the two fields being unrelated (2.5% of the analyses should be both positively and negatively correlated on average). However, the analyses with positive correlations are higher than what one would expect by about 10.9%. We also tested whether our conclusions changed when using different parameters of the localization windows. (The same criterion was used as in the baseline analysis where 99% of the window's power is concentrated within the region of interest.) As shown in Table 1, the regions that are negatively correlated do not depend upon the parameters of the localization windows. The percentage of the analyses that are positively correlated, however, does increase from 5.0% for windows with angular radii of 6° to about 18.4% for localization windows with radii of 12°. Regardless, the conclusions of our analysis remain unchanged: The negative correlations are always consistent with being random, whereas the positive correlations are in excess of what one would expect for unrelated fields.

Results for the correlation between the total free-air gravity and the magnetic field strength are shown in the lower left panel of Figure 3 and in Table 1. These results are seen to be nearly identical to those obtained using

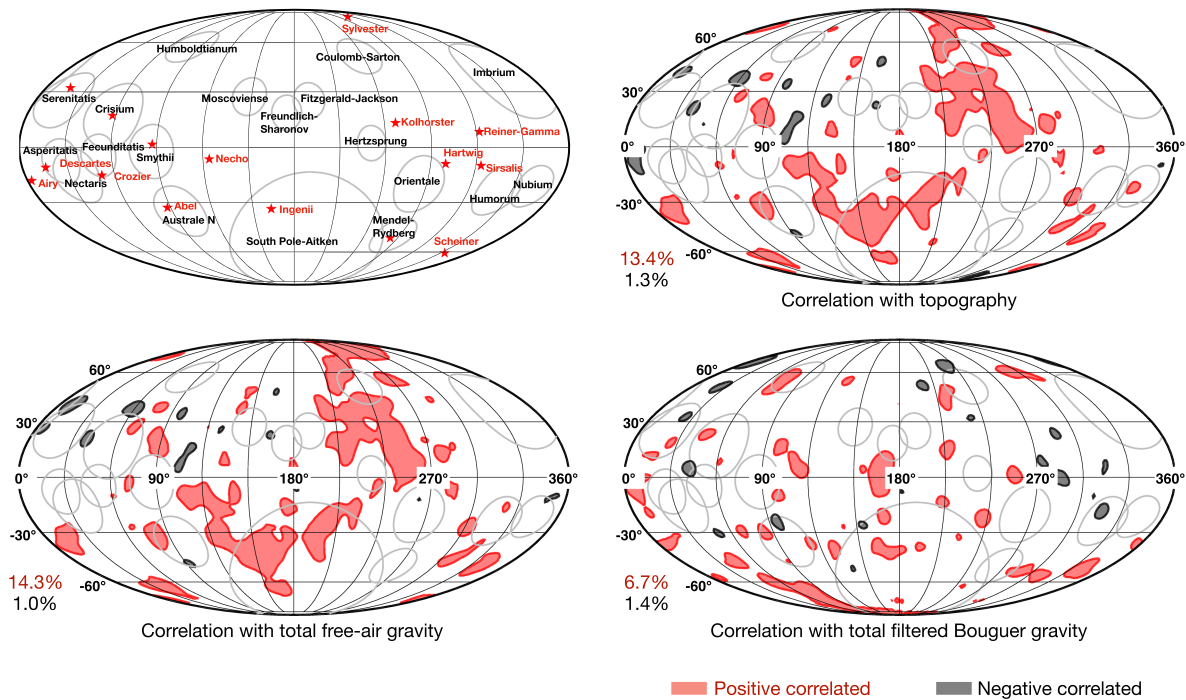


Figure 3. Regions where the average spectral correlation exceeds the 95% confidence limits. Positive correlations are contoured in red, and negative correlations are contoured in black. The upper left image provides context by plotting the impact basins that are greater than 500 km in diameter in gray (Neumann et al., 2015) with their names in black, and the locations of some of the prominent magnetic anomalies are shown as red stars with their associated names. When the anomaly is named after the impact basin, its name is shown in black. The other three panels show results using the (upper right) topography, (lower left) total free-air gravity, and (lower right) total modified Bouguer gravity. All maps are presented in a Mollweide equal-area projection and centered on the farside. The percentages noted in the bottom left of each image correspond to the percentage of the lunar surface with positive (red) and negative (black) correlations that exceed the 95% confidence limits.

the topography. The reason for this is that lunar free-air gravity is highly correlated with surface topography for short wavelengths. In fact, for degrees greater than 80, the correlation between free-air gravity and gravity predicted from topography is usually greater than 0.98 (Lemoine et al., 2014).

Our correlation results between the total modified Bouguer gravity and total magnetic field intensity are shown in the lower right panel of Figure 3. In this case, we found that only 8.1% of the surface area of the Moon has average correlations that exceed the 95% confidence limits, and this is just slightly larger than the 5% that would be expected to occur if the magnetic field intensity and total modified Bouguer anomaly were unrelated. Of the 8.1% of the region that has $|\bar{\gamma}|$ larger than $|\bar{\gamma}_{95}|$, 6.7% corresponds to positive correlations and 1.4% corresponds to negative correlations. Thus, the regions with negative correlations that exceeded the 95% confidence limits are consistent with the two fields being unrelated, just as was the case

Table 1
Percentage of the Moon's Surface Area Where $|\bar{\gamma}| > |\bar{\gamma}_{95}|$

Localized window parameters	Topography		Total free-air gravity		Total modified Bouguer gravity	
	Positive	Negative	Positive	Negative	Positive	Negative
$\theta = 6^\circ, l_{\text{win}} = 43, K = 1$	5.0%	1.8%	5.4%	1.6%	3.5%	1.9%
$\theta = 8^\circ, l_{\text{win}} = 32, K = 1$	9.0%	1.7%	9.8%	1.3%	5.1%	1.9%
$\theta = 10^\circ, l_{\text{win}} = 26, K = 1$	13.4%	1.3%	14.3%	1.0%	6.7%	1.4%
$\theta = 12^\circ, l_{\text{win}} = 21, K = 1$	18.4%	1.1%	20.2%	0.7%	9.2%	0.8%
$\theta = 10^\circ, l_{\text{win}} = 35, K = 3$	13.2%	1.5%	14.4%	1.2%	7.3%	2.2%

Note. Results are shown using several different localization windows parameters (where θ is the angular radius of the window, l_{win} is the spectral bandwidth of the window, and K is the number of tapers used in the analysis). For each field, the percentages of the correlations that are positive and negative are indicated. For random fields, the positive and negative correlations would be expected to be about 2.5% each.

with our analyses that considered topography and total free-air gravity. However, the analyses with positive correlations are slightly higher than what one would expect by about 4.2%, which seems to indicate that in a few cases, the total modified Bouguer gravity might be correlated with the total field intensity. Similar results are obtained when using single localization windows with radii that range from 6° to 12° or multitaper analyses with three localization windows (see Table 1).

The above analyses used a minimum degree of $l_1 = 3l_{\text{win}}$, and we tested the sensitivity of the results to this choice. By increasing the minimum degree to $4l_{\text{win}}$, the results are generally consistent with those discussed above, but there are slightly fewer regions where the total field intensity is positively correlated with either topography, total free-air gravity, or total modified Bouguer gravity (see Figure S1 in the supporting information). For example, the surface area that possesses statistically significant positive correlations using topography is decreased slightly from 13.4% to 10.3%. For the results of using total free-air gravity and total modified Bouguer gravity, the surface area reduced somewhat from 14.3% to 11.8% and from 6.7% to 6.0%, respectively.

We next tested the sensitivity of our results by performing the correlation analyses at 30 km altitude, which corresponds to where most of the magnetic field measurements were obtained. These results are shown in Figure S2 in the supporting information. When using topography, the surface area that has average correlations greater than the 95% confidence limits decreased by nearly a factor of 2 compared to those at the surface, from a total of about 15% to 8%. Regardless, the regions that are negatively correlated are still consistent with not being statistically significant, and those regions that are positively correlated exceed that expected of unrelated fields by about 3–4% of the Moon's surface area. The results of using the total free-air gravity are nearly identical to those of using topography. For the results using the total modified Bouguer gravity, the surface area decreased from 8.1% to 5.3%, with the negative correlations remaining consistent with being random. The correlation results are thus somewhat sensitive to the altitude at which the analysis is performed, and this is simply because the magnetic field intensity is sensitive to the magnetization direction and is not always centered directly over the magnetic sources. Simulations using magnetized disks show that there can be an offset between the strongest magnetic field intensity and the location of the magnetic sources and that this offset increases with altitude. Thus, by performing a correlation analysis at spacecraft altitudes, one would naturally expect the correlations between the magnetic field and other observables to decrease, as is observed.

We also tested the sensitivity of our results by using the 99.7% (3σ) confidence limits instead of the 95% (2σ) confidence limits. As shown in Figure S3, the regions that have an average correlation value that is negative and that is greater than the 99.7% confidence limits only cover less than 0.15% of the surface area. Thus, both the 95% and 99.7% confidence limits show that the regions with negative correlations are consistent with being uncorrelated. On the other hand, the percentages of the areas that have a positive correlation that is greater than the 99.7% confidence limit are 4.2%, 4.8%, and 1.1% when using the topography, total free-air gravity, and total modified Bouguer gravity, respectively. Similar to when using the 95% confidence limits, this shows that more regions are positively correlated than one would expect by chance.

Up until this point, when analyzing the correlations between the various data sets, we have made use of the magnetic field intensity given that it is less sensitive to the direction of magnetization than any of its three vector components and its potential. Nevertheless, we have investigated how our correlation results depend upon using both the potential and radial components of both the magnetic and gravity fields.

We find that the radial modified Bouguer gravity shows no statistical correlation with the radial component of the magnetic field. Both topography and the radial free-air gravity also show no statistical correlation with the radial component of the magnetic field. The results of using magnetic and gravitational potentials are nearly identical to those of using the radial components of the magnetic and gravity fields (i.e., there is no statistically significant correlation). Thus, no statistically significant correlations were found using either the potential or the radial components of the magnetic and gravity fields. These results are easily understood. An isolated magnetic source will generate both positive and negative magnetic anomalies when using only a single vector component. When calculating correlations with another field over a large region, the negative and positive components of the magnetic field average to zero.

We also tested our results by using a different statistical metric. Instead of using the average correlation, we tested the use of the average of the absolute value of the correlation. The results were found to be not too

different with respect to those discussed above, with the exception that the sign information in the correlation was discarded. Additional statistical metrics could conceivably be tested as well, including weighted averages and quadratic estimates.

Lastly, we have also performed our correlation analysis in the spatial domain. Spatial maps of the gravity, topography, and magnetic field were first obtained on a regularly spaced grid, and the maps were constructed using the same spherical harmonic degree ranges as in the spectral analyses. For a specified location, data were sampled within a circle, whose size corresponded to the same radii as in our spectral analyses. The correlation between the two data sets was then computed, ensuring that each pixel was weighted by its corresponding area. However, as expected, we found that the correlation results were highly sensitive to the degree ranges that were used when constructing the gridded data. For example, we found that 57.3% of our analyses had correlations that were larger than the 95% confidence limits (44.5% positively and 12.8% negatively) when using the entire degree range of the magnetic field intensity and total free-air gravity. Whereas, by removing the first $3l_{\text{win}}$ and last $2l_{\text{win}}$ degrees, only 18% of the surface area exceeded the 95% limits (16.9% positively and 1.1% negatively), which is consistent with the results obtained in the spectral domain. Similar behavior was found when using the topography: The surface area decreased from 62.9% to 17.3% by using the degrees from $3l_{\text{win}}$ to $l_{\text{max}} - 2l_{\text{win}}$, with 16.4% possessing positive correlations and 0.9% possessing negative correlations. For the results using total modified Bouguer gravity, the surface areas decreased from 21% to 11% by removing the first $3l_{\text{win}}$ and the last $2l_{\text{win}}$ degrees.

4. Discussion

The origin of lunar magnetic anomalies is a long-standing enigmatic topic in lunar science, and in this study, we have attempted to place constraints on their origin by investigating whether they are correlated with gravity or topography. Using a localized cross-spectral analysis, our results show that there are no statistically significant negative correlations between the magnetic field intensity and topography, the total free-air gravity, or the total modified Bouguer gravity. Depending on the analysis parameters, the surface area of the Moon with statistically significant positive correlations between the magnetic field intensity and both topography and the total free-air gravity exceeds that expected for unrelated fields by up to 18%. For the case of the total modified Bouguer gravity and magnetic field intensity, the surface area with statistically significant positive correlations exceeds that for unrelated fields by up to 7%.

We first discuss our results concerning the total modified Bouguer gravity, which is related to subsurface density anomalies. The first result is that there are no statistically significant negative correlations between the total magnetic field and total modified Bouguer gravity. This means that there are no cases where a region of the crust with a negative density anomaly would cause a positive enhancement in magnetic field strength (or the converse). The statistically significant correlations that are found are thus a result of positive density anomalies causing positive magnetic intensity anomalies, or conversely, negative density anomalies causing a reduction in the magnetic field intensity.

The regions that do possess positive correlations between the total modified Bouguer gravity and magnetic field intensity are relatively few, isolated, and small in total area. It is thus somewhat difficult to determine which regions occur by chance as opposed to those that are a result of a real correlation between subsurface density anomalies and crustal magnetization. To elucidate the origin of these positive correlations, we first compared these regions to the linear gravity anomalies identified in the Bouguer gravity by Andrews-Hanna et al. (2013) but did not find any clear association. Wiczorek (2018) showed that the vast majority of crustal magnetization was located in the deep crust (several kilometers below the surface), and it is thus surprising that there are not more regions with statistically significant positive correlations between the magnetic field intensity and the total modified Bouguer gravity. Together, these results imply that the majority of deep magnetization in the crust of the Moon is not associated with a detectable density contrast.

The lack of a more substantial correlation between deep magnetization and subsurface density anomalies could be accounted for by one of four scenarios. First, if these magnetic anomalies were the result of magmatic intrusions, they would need to have the same density as the anorthositic crust that they intruded. This seems unlikely, given that basaltic magmas and Mg-suite intrusive rocks are considerably more mafic (and hence denser) than anorthositic rocks. Second, it is possible that the deep crust has a uniform composition but that it cooled heterogeneously in time. If the core dynamo strength varied in intensity and/or direction during cooling, this could have led to variations in deep crustal magnetization. The entire

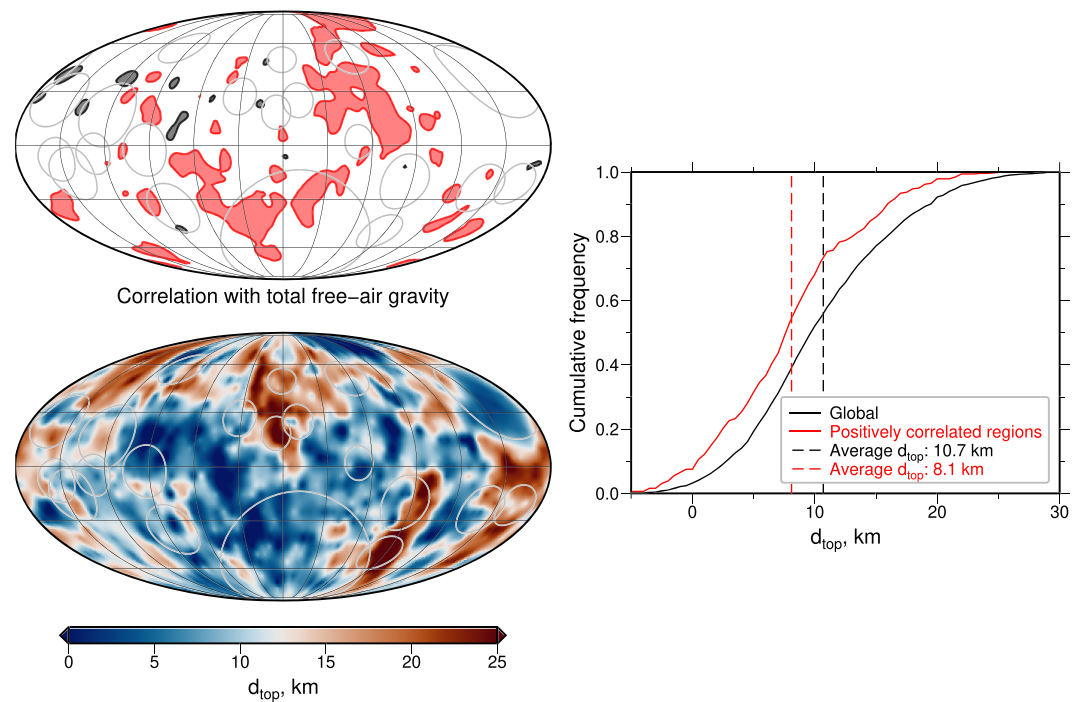


Figure 4. (upper left) Correlation between the total free-air gravity and magnetic field intensity calculated at the surface, (lower left) depth to the top of the magnetic sources from Wiczorek (2018), and (right) the cumulative frequency of the depth to the top of the magnetic sources globally (black) and within only those regions with statistically significant positive correlations between free-air gravity and magnetic field intensity (red).

crust is expected to cool below the Curie temperature of iron metal in the first 100 Myr of lunar evolution (Laneuville et al., 2018), so this would require temporal variations in magnetic field strength and cooling rates during the earliest part of lunar evolution. Third, it is possible that small variations in iron-metal content in the deep crust are responsible for lateral variations in magnetic field strength but that the resulting density anomalies are sufficiently small to be undetectable in the gravity data. For example, magnetized lunar rocks typically contain about 1 wt.% Fe metal (e.g., Fuller & Cisowski, 1987), and the addition of 1 wt.% metal to an anorthositic rock would only increase its bulk density by about 16 kg m^{-3} . Given that the GRAIL bulk density estimates have uncertainties of the same order (Besserer et al., 2014; Wiczorek et al., 2013), it is unlikely that such small variations in iron metal content would be discernible in the modified Bouguer gravity. Lastly, if the magnetization is associated with density anomalies located deep within the crust, it is possible that the obtained correlation would be relatively small since the correlation results are sensitive to the depth of the magnetic sources.

In contrast to the modified Bouguer gravity, both the free-air gravity and topography show substantial enhancements in the percentage of the Moon's surface area that have higher correlations with the magnetic field intensity than expected by chance. Like the results with the modified Bouguer anomaly, we first find that there are no statistically significant negative correlations between magnetic field intensity and either the free-air gravity or topography. This means that there are no cases where enhancements in the magnetic field intensity are associated with lower elevations or lower free-air gravity anomalies. Thus, enhancements in the magnetic field intensity are statistically associated with higher elevations with higher free-air gravities (or the converse). The behaviors of the free-air gravity and topography are nearly identical, and this is because the free-air gravity is almost entirely a result of variations in topography.

These results suggest that the regions with high positive correlations are the result of the addition of magnetized materials on to the top of the lunar crust. Crustal magnetization for these regions would thus be expected to be close to the surface. To test this hypothesis, we first investigated how the depths of magnetization derived by Wiczorek (2018) compare with our regions with statistically significant correlations. In Figure 4 we plot the correlation results using total free-air gravity and magnetic field intensity in the upper left panel and the depth to the top of the magnetic sources from Wiczorek (2018) in the lower left

panel. In the right panel of this figure we plot the cumulative frequency of the depth of magnetic sources for the entire Moon (black) and the cumulative frequency only for those regions with statistically significant positive correlations (red). The average depth to the top of the magnetized regions for the entire Moon is found to be 10.7 km, whereas when considering only those regions with statistically significant correlations between magnetic field strength and free-air gravity the average depth is 8.1 km. Thus, crustal magnetization is closer to the surface wherever the magnetic field strength and free-air gravity (or topography) are statistically correlated. Examples where both the depth to magnetization is shallow and the magnetic field strength is statistically correlated with free-air gravity include regions within the northern portion of the South Pole-Aitken basin, which extend to the north-west and north-east beyond the rim, as well as parts of the region north of the Orientale basin.

We also compared our results with the distribution of lunar swirls, which likely have extremely shallow source depths as shown in the study of Hemingway and Tikoo (2018). As shown in Figure S4, we found that more than half of the swirls as mapped by Denevi et al. (2016) are within or are proximal to our high correlation regions. For example, a large portion of the lunar swirls are located in the northern portion of the South Pole-Aitken basin. Another region is northeast of the Smythii basin, where some, but not all, of the swirls in this region are associated with high correlations. We note that there is no obvious relation between the regions with statistically significant correlations and either the composition of the surface, surface age, or surface geomorphology.

The most plausible explanation for the regions with shallow depths of magnetization and statistically significant correlations between magnetic field intensity and free-air gravity is that they are related to the emplacement of impact basin ejecta on the surface that contain small quantities of iron metal derived from the impactor (see Wiczorek et al., 2012). For example, one extensive region is found in the northern portion of the South Pole-Aitken basin. This region possesses some of the strongest magnetic anomalies on the Moon and was previously suggested by Wiczorek et al. (2012) to be the result of iron-rich remnants of the projectile that formed this basin that were subsequently magnetized in the presence of a core-generated dynamo field. The northwest and northeast extension of this region is consistent with the deposition of projectile materials from an oblique impact from south to north as suggested by Garrick-Bethell and Zuber (2009). Another notable region is located north of the Orientale impact basin that extends almost to the north pole of the Moon.

A large portion of the high correlation regions also possess strong magnetic field intensities at the surface (Figure S5). For example, if we take 50 nT as a threshold magnetic field strength, almost half of these high magnetic field regions show statistically significant positive correlations with total free-air gravity. In Figure S5 we also plot the distribution of mare basalts as mapped by Nelson et al. (2014). These are located primarily on the nearside in a region where the magnetic field intensities are extremely weak (see Wiczorek, 2018). This image shows that the regions with statistically significant correlations between the magnetic field and free-air gravity are not associated with mare basalts. Finally, we also note that almost no regions have statistically significant correlations between magnetic field intensity and either free-air gravity or topography within the Procellarum KREEP Terrane (Jolliff et al., 2000) on the nearside of the Moon. The magnetic field strengths are extremely weak in this region which is plausibly explained by the local high heat production and delayed cooling below the Curie temperature of iron metal until after the core dynamo shut off (Laneuville et al., 2018).

5. Conclusion

We used a localized cross-spectral analysis to test whether the magnetic anomalies on the Moon are correlated with gravity or topography. Our results show that there are no regions that have statistically significant negative correlations between the magnetic field intensity and free-air gravity, topography, or modified Bouguer gravity. Portions of the surface do show statistically significant positive correlations with free-air gravity and topography and also in a small number of cases with the modified Bouguer gravity. The regions that show statistically significant positive correlations with free-air gravity and topography are likely to have shallow depths of magnetization and could be related to iron-rich impact ejecta. The regions that are statistically correlated, however, are rather small in area: up to about 18% for the free-air gravity or topography

and 7% for the modified Bouguer gravity. Although the origin of most lunar magnetic anomalies remains enigmatic, our work elucidates the origin of the strongest magnetic anomalies on the Moon.

Acknowledgments

We thank Michael Sori and two anonymous reviewers for their valuable and insightful comments that helped us improve the manuscript. This work was supported by the National Natural Science Foundation of China (11803066), the French Space Agency (CNES), and a Chinese Academy of Sciences Scholarship. The GRAIL gravity data are available at the Planetary Data System (<https://pds-geosciences.wustl.edu>), LOLA data can be found in Wieczorek (2007), and the magnetic field model can be download online (at <https://jlpeda.jaxa.jp/globalSVM20150511.zip>). Data plotted in Figures 2, 3, and S1 to S3 can be download from Gong and Wieczorek (2020).

References

- Andrews-Hanna, J. C., Asmar, S. W., Head, J. W., Kiefer, W. S., Konopliv, A. S., Lemoine, F. G., et al. (2013). Ancient igneous intrusions and early expansion of the Moon revealed by GRAIL gravity gradiometry. *Science*, 339(6120), 675–678. <https://doi.org/10.1126/science.1231753>
- Besserer, J., Nimmo, F., Wieczorek, M. A., Weber, R. C., Kiefer, W. S., McGovern, P. J., et al. (2014). GRAIL gravity constraints on the vertical and lateral density structure of the lunar crust. *Geophysical Research Letters*, 41, 5771–5777. <https://doi.org/10.1002/2014GL060240>
- Cébron, D., Laguerre, R., Noir, J., & Schaeffer, N. (2019). Precessing spherical shells: flows, dissipation, dynamo and the lunar core. *Geophysical Journal International*, 219, S34–S57. <https://doi.org/10.1093/gji/ggz037>
- Denevi, B. W., Robinson, M. S., Boyd, A. K., Blewett, D. T., & Klima, R. L. (2016). The distribution and extent of lunar swirls. *Icarus*, 273, 53–67. <https://doi.org/10.1016/j.icarus.2016.01.017>
- Dwyer, C. A., Stevenson, D. J., & Nimmo, F. (2011). A long-lived lunar dynamo driven by continuous mechanical stirring. *Nature*, 479, 212–214. <https://doi.org/10.1038/nature10564>
- Dyal, P., Parkin, C. W., & Daily, W. D. (1974). Magnetism and the interior of the Moon. *Reviews of Geophysics*, 12, 568–591. <https://doi.org/10.1029/RG012i004p00568>
- Evans, A. J., Zuber, M. T., Weiss, B. P., & Tikoo, S. M. (2014). A wet, heterogeneous lunar interior: Lower mantle and core dynamo evolution. *Journal of Geophysical Research: Planets*, 119, 1061–1077. <https://doi.org/10.1002/2013JE004494>
- Fuller, M., & Cisowski, S. M. (1987). Lunar paleomagnetism. *Geomagnetism*, 2, 307–455.
- Garrick-Bethell, I., & Kelley, M. R. (2019). Reiner Gamma: A magnetized elliptical disk on the Moon. *Geophysical Research Letters*, 46, 5065–5074. <https://doi.org/10.1029/2019GL082427>
- Garrick-Bethell, I., Weiss, B. P., Shuster, D. L., & Buz, J. (2009). Early lunar magnetism. *Science*, 323, 356–359. <https://doi.org/10.1126/science.1166804>
- Garrick-Bethell, I., Weiss, B. P., Shuster, D. L., Tikoo, S. M., & Tremblay, M. M. (2017). Further evidence for early lunar magnetism from troctolite 76535. *Journal of Geophysical Research: Planets*, 122, 76–93. <https://doi.org/10.1002/2016JE005154>
- Garrick-Bethell, I., & Zuber, M. T. (2009). Elliptical structure of the lunar South Pole-Aitken basin. *Icarus*, 204, 399–408. <https://doi.org/10.1016/j.icarus.2009.05.032>
- Gong, S., & Wieczorek, M. A. (2020). Is the lunar magnetic field correlated with gravity or topography? *Journal of Geophysical Research: Planets*. <https://doi.org/10.5281/zenodo.3630535>
- Halekas, J. S., Mitchell, D. L., Lin, R. P., Frey, S., Hood, L. L., Acuña, M. H., & Binder, A. B. (2001). Mapping of crustal magnetic anomalies on the lunar near side by the Lunar Prospector electron reflectometer. *Journal of Geophysical Research*, 106, 27,841–27,852. <https://doi.org/10.1029/2000JE001380>
- Hemingway, D. J., & Tikoo, S. M. (2018). Lunar swirl morphology constrains the geometry, magnetization, and origins of lunar magnetic anomalies. *Journal of Geophysical Research: Planets*, 123, 2223–2241. <https://doi.org/10.1029/2018JE005604>
- Hood, L. L. (2011). Central magnetic anomalies of Nectarian-aged lunar impact basins: Probable evidence for an early core dynamo. *Icarus*, 211, 1109–1128. <https://doi.org/10.1016/j.icarus.2010.08.012>
- Hood, L. L., & Artemieva, N. A. (2008). Antipodal effects of lunar basin-forming impacts: Initial 3D simulations and comparisons with observations. *Icarus*, 193, 485–502. <https://doi.org/10.1016/j.icarus.2007.08.023>
- Hood, L. L., Zakharian, A., Halekas, J., Mitchell, D. L., Lin, R. P., Acuña, M. H., & Binder, A. B. (2001). Initial mapping and interpretation of lunar crustal magnetic anomalies using Lunar Prospector magnetometer data. *Journal of Geophysical Research*, 106, 27,825–27,839. <https://doi.org/10.1029/2000JE001366>
- Jansen, J., Andrews-Hanna, J., Li, Y., Lucey, P., Taylor, G., Goossens, S., et al. (2017). Small-scale density variations in the lunar crust revealed by GRAIL. *Icarus*, 291, 107–123. <https://doi.org/10.1016/j.icarus.2017.03.017>
- Jolliffe, B. L., Gillis, J. J., Haskin, L. A., Korotev, R. L., & Wieczorek, M. A. (2000). Major lunar crustal terranes: Surface expressions and crust-mantle origins. *Journal of Geophysical Research*, 105(E2), 4197–4216. <https://doi.org/10.1029/1999JE001103>
- Konrad, W., & Spohn, T. (1997). Thermal history of the Moon: Implications for an early core dynamo and post-accretionary magmatism. *Advances in Space Research*, 19, 1511–1521. [https://doi.org/10.1016/S0273-1177\(97\)00364-5](https://doi.org/10.1016/S0273-1177(97)00364-5)
- Laneuville, M., Taylor, J., & Wieczorek, M. A. (2018). Distribution of radioactive heat sources and thermal history of the Moon. *Journal of Geophysical Research: Planets*, 123, 3144–3166. <https://doi.org/10.1029/2018JE005742>
- Laneuville, M., Wieczorek, M. A., Breuer, D., Aubert, J., Morard, G., & Ruckriemen, T. (2014). A long-lived lunar dynamo powered by core crystallization. *Earth and Planetary Science Letters*, 401, 251–260. <https://doi.org/10.1016/j.epsl.2014.05.057>
- Le Bars, M., Wieczorek, M. A., Karatekin, Ö., Cébron, D., & Laneuville, M. (2011). An impact-driven dynamo for the early Moon. *Nature*, 479, 215–218. <https://doi.org/10.1038/nature10565>
- Lemoine, F. G., Goossens, S., Sabaka, T. J., Nicholas, J. B., Mazarico, E., Rowlands, D. D., et al. (2014). GRGM900C: A degree 900 lunar gravity model from GRAIL primary and extended mission data. *Geophysical Research Letters*, 41, 3382–3389. <https://doi.org/10.1002/2014GL060027>
- Mighani, S., Wang, H., Shuster, D. L., Borlina, C. S., Nichols, C. I. O., & Weiss, B. P. (2020). The end of the lunar dynamo. *Science Advances*, 6, eaax0883.
- Milbury, C. A., Smrekar, S. E., Raymond, C. A., & Schubert, G. (2007). Lithospheric structure in the eastern region of Mars' dichotomy boundary. *Planetary and Space Science*, 55, 280–288. <https://doi.org/10.1016/j.pss.2006.03.009>
- Nelson, D. M., Koeber, S. D., Daud, K., Robinson, M. S., Watters, T. R., Banks, M. E., & Williams, N. R. (2014). Mapping lunar maria extents and lobate scarps using LROC image products. In *Proc. Lunar Planet. Sci. Conf* (pp. 2861).
- Neumann, G. A., Zuber, M. T., Wieczorek, M. A., Head, J. W., Baker, D. M. H., Solomon, S. C., et al. (2015). Lunar impact basins revealed by Gravity Recovery and Interior Laboratory measurements. *Science Advances*, 1, e1500852. <https://doi.org/10.1126/sciadv.1500852>
- Oliveira, J. S., Wieczorek, M. A., & Kletetschka, G. (2017). Iron abundances in lunar impact basin melt sheets from orbital magnetic field data. *Journal of Geophysical Research: Planets*, 122, 2429–2444. <https://doi.org/10.1002/2017JE005397>
- Purucker, M. E., Head, J. W., & Wilson, L. (2012). Magnetic signature of the lunar South Pole-Aitken basin: Character, origin, and age. *Journal of Geophysical Research*, 117, E05001. <https://doi.org/10.1029/2011JE003922>
- Scheinberg, A. L., Soderlund, K. M., & Elkins-Tanton, L. T. (2018). A basal magma ocean dynamo to explain the early lunar magnetic field. *Earth and Planetary Science Letters*, 492, 144–151. <https://doi.org/10.1016/j.epsl.2018.04.015>

- Scheinberg, A. L., Soderlund, K. M., & Schubert, G. (2015). Magnetic field generation in the lunar core: The role of inner core growth. *Icarus*, 254, 62–71. <https://doi.org/10.1016/j.icarus.2015.03.013>
- Simons, F. J., Dahlen, F. A., & Wiczeorek, M. A. (2006). Spatiospectral concentration on a sphere. *SIAM Review*, 48, 504–536. <https://doi.org/10.1137/S0036144504445765>
- Smith, D. E., Zuber, M. T., Neumann, G. A., Lemoine, F. G., Mazarico, E., Torrence, M. H., et al. (2010). Initial observations from the Lunar Orbiter Laser Altimeter (LOLA). *Geophysical Research Letters*, 37, L18204. <https://doi.org/10.1029/2010GL043751>
- Smrekar, S. E., McGill, G. E., Raymond, C. A., & Dimitriou, A. M. (2004). Geologic evolution of the Martian dichotomy in the Ismenius area of Mars and implications for plains magnetization. *Journal of Geophysical Research*, 109, E11002. <https://doi.org/10.1029/2004JE002260>
- Suavet, C., Weiss, B. P., Cassata, W. S., Shuster, D. L., Gattacceca, J., Chan, L., et al. (2013). Persistence and origin of the lunar core dynamo. *Proceedings of the National Academy of Sciences of the United States of America*, 110, 8453–8458. <https://doi.org/10.1073/pnas.1300341110>
- Thorey, C., Michaut, C., & Wiczeorek, M. (2015). Gravitational signatures of lunar floor-fractured craters. *Earth and Planetary Science Letters*, 424, 269–279. <https://doi.org/10.1016/j.epsl.2015.04.021>
- Tikoo, S. M., Weiss, B. P., Cassata, W. S., Shuster, D. L., Gattacceca, J., Lima, E. A., et al. (2014). Decline of the lunar core dynamo. *Earth and Planetary Science Letters*, 404, 89–97. <https://doi.org/10.1016/j.epsl.2014.07.010>
- Tikoo, S. M., Weiss, B. P., Shuster, D. L., Suavet, C., Wang, H., & Grove, T. L. (2017). A two-billion-year history for the lunar dynamo. *Science Advances*, 3, E1700207. <https://doi.org/10.1126/sciadv.1700207>
- Tsunakawa, H., Shibuya, H., Takahashi, F., Shimizu, H., Matsushima, M., Matsuoka, A., et al. (2010). Lunar magnetic field observation and initial global mapping of lunar magnetic anomalies by MAP-LMAG onboard SELENE (Kaguya). *Space Science Reviews*, 154, 219–251. <https://doi.org/10.1007/s11214-010-9652-0>
- Tsunakawa, H., Takahashi, F., Shimizu, H., Shibuya, H., & Matsushima, M. (2015). Surface vector mapping of magnetic anomalies over the Moon using Kaguya and Lunar Prospector observations. *Journal of Geophysical Research: Planets*, 120, 1160–1185. <https://doi.org/10.1002/2014JE004785>
- Weiss, B. P., & Tikoo, S. M. (2014). The lunar dynamo. *Science*, 346, 1246753. <https://doi.org/10.1126/science.1246753>
- Wiczeorek, M. A. (2007). Spherical harmonic models of planetary topography. <https://doi.org/10.5281/zenodo.997406>
- Wiczeorek, M. A. (2015). Gravity and topography of the terrestrial planets. In G. Schubert (Ed.), *Treatise on geophysics* (pp. 153–193). Oxford: Elsevier. <https://doi.org/10.1016/B978-0-444-53802-4.00169-X>
- Wiczeorek, M. A. (2018). Strength, depth, and geometry of magnetic sources in the crust of the Moon from localized power spectrum analysis. *Journal of Geophysical Research: Planets*, 123, 291–316. <https://doi.org/10.1002/2017JE005418>
- Wiczeorek, M. A., & Meschede, M. (2018). SHTools: Tools for working with spherical harmonics. *Geochemistry, Geophysics, Geosystems*, 19, 2574–2592. <https://doi.org/10.1029/2018GC007529>
- Wiczeorek, M. A., Neumann, G. A., Nimmo, F., Kiefer, W. S., Taylor, J. G., Melosh, J. H., et al. (2013). The crust of the Moon as seen by GRAIL. *Science*, 339, 671–675. <https://doi.org/10.1126/science.1231530>
- Wiczeorek, M. A., & Simons, F. J. (2005). Localized spectral analysis on the sphere. *Geophysical Journal International*, 162, 655–675. <https://doi.org/10.1111/j.1365-246X.2005.02687.x>
- Wiczeorek, M. A., & Simons, F. J. (2007). Minimum-variance multitaper spectral estimation on the sphere. *Journal of Fourier Analysis and Applications*, 13, 665–692. <https://doi.org/10.1007/s00041-006-6904-1>
- Wiczeorek, M. A., Weiss, B. P., & Stewart, S. T. (2012). An impactor origin for lunar magnetic anomalies. *Science*, 335, 1212–1215. <https://doi.org/10.1126/science.1214773>
- Wiczeorek, M. A., Zuber, M. T., & Phillips, R. J. (2001). The role of magma buoyancy on the eruption of lunar basalts. *Earth and Planetary Science Letters*, 185, 71–83. [https://doi.org/10.1016/S0012-821X\(00\)00355-1](https://doi.org/10.1016/S0012-821X(00)00355-1)
- Zuber, M. T., Smith, D. E., Watkins, M. M., Asmar, S. W., Konopliv, A. S., Lemoine, F. G., et al. (2013). Gravity field of the Moon from the Gravity Recovery and Interior Laboratory (GRAIL) mission. *Science*, 339, 668–671. <https://doi.org/10.1126/science.1231507>